Ocean Engineering 220 (2021) 108407

Contents lists available at ScienceDirect

Ocean Engineering

journal homepage: www.elsevier.com/locate/oceaneng

Vessel hydrodynamic model tuning by Discrete Bayesian updating using simulated onboard sensor data

Xu Han [a,b,*], Bernt Johan Leira [a,b], Svein Sævik [a,b]

[a] Department of Marine Technology, Norwegian University of Science and Technology (NTNU), 7491, Trondheim, Norway
[b] Centre for Research-based Innovation on Marine Operations (SFI MOVE), Norway

ARTICLE INFO

Keywords:
Tuning of seakeeping model
Wave-induced vessel responses
Sensor signal processing
Discrete Bayesian updating
Inverse distance weighting
Sensitivity studies
Validation analysis

ABSTRACT

Vessel and wave hydrodynamics are fundamental for vessel motion prediction. Improving hydrodynamic model accuracy without compromising computational efficiency has always been of high interest for safe and cost-effective marine operations. With continuous development of sensor technology and computational capacity, an improved digital twin concept for vessel motion prediction can be realized based on an onboard online adaptive hydrodynamic model. This article proposes and demonstrates a practical approach for tuning of important vessel hydrodynamic model parameters based on simulated onboard sensor data of vessel motion response. The algorithm relies fundamentally on spectral analysis, probabilistic modelling and the discrete Bayesian updating formula. All case studies show promising and reasonable tuning results. Sensitivities of the approach with respect to its key parameters were also studied. Sensor noise has been considered. The algorithm is found to be computationally efficient, robust and stable when tuning the values of hydrodynamic parameters and updating their uncertainties, within reasonable sensor noise levels.

1. Introduction

The energy sector is experiencing rapid change with a fast growth in offshore wind and solar farms, an increased number of subsea installations to provide tie-backs to existing oil and gas facilities as well as a continuous drive towards exploration of natural resources in deeper and colder ocean areas. These trends lead to more challenging marine operations, facing heavier offshore lifts, more complex operation systems, and severe operational environments. Hence, the economic incentives for obtaining broader operational weather windows by reducing the inherent uncertainties of marine operations increase. As of today, engineering practice considers uncertainties conservatively and marine operations are designed and simulated according to rules (e.g., DNVGL-ST-N001 (2016)) before they are executed. Uncertainty reduction in vessel seakeeping analysis has been focused on by both industry and research institutions for decades. Knowledge on modelling of wave and vessel hydrodynamics has been rather well developed, with respect to engineering practice (Faltinsen, 1990; DNVGL-RP-C205, 2017). In principle one can design the marine operation by application of the most computational demanding and accurate hydrodynamic models, e.g., by including nonlinear wave kinematics (Yue et al., 2008; Nouguier et al., 2014) and vessel hydrodynamics (Cao et al., 2010; Larsen et al., 2019; Himeno, 1981; Faltinsen, 2015), and even by applying computational fluid dynamics (CFD) (Kim, 2011).

However, the on-site uncertainties related to wave and vessel condition may reduce the value of engineering efforts during the design phase. Instead of applying very high fidelity models in the operation design phase to increase the accuracy (e.g., by using nonlinear or CFD programs), a lot of efforts have been made on increasing the knowledge of the on-site wave forecast and real-time vessel operational condition. With the development in sensor technology and computational process capacity during the last two decades, many research-oriented onboard decision support systems (ODSS) for marine and offshore activities have been developed aiming at improving vessel motion predictions. Examples are: 1) SeaSense system (Nielsen et al., 2006); 2) CASH system (Clauss et al., 2012); 3) OWME project (Onboard Wave and Motion Estimator) applying non-coherent WaMoS II radar (Dannenberg et al., 2010; Naaijen et al., 2016, 2018); 4) ESMF project (Environment and Ship Motion Forecasting) applying coherent wave radar systems (Connell et al., 2015; Kusters et al., 2016; Alford et al., 2015). On-site full-scale tests have been performed for validation of the different proposed methods (Naaijen et al., 2016, 2018; Connell et al., 2015; Alford et al.,

* Corresponding author. Department of Marine Technology, Norwegian University of Science and Technology (NTNU), 7491, Trondheim, Norway.
E-mail address: xu.han@ntnu.no (X. Han).

https://doi.org/10.1016/j.oceaneng.2020.108407
Received 30 April 2020; Received in revised form 21 September 2020; Accepted 22 November 2020
Available online 9 December 2020

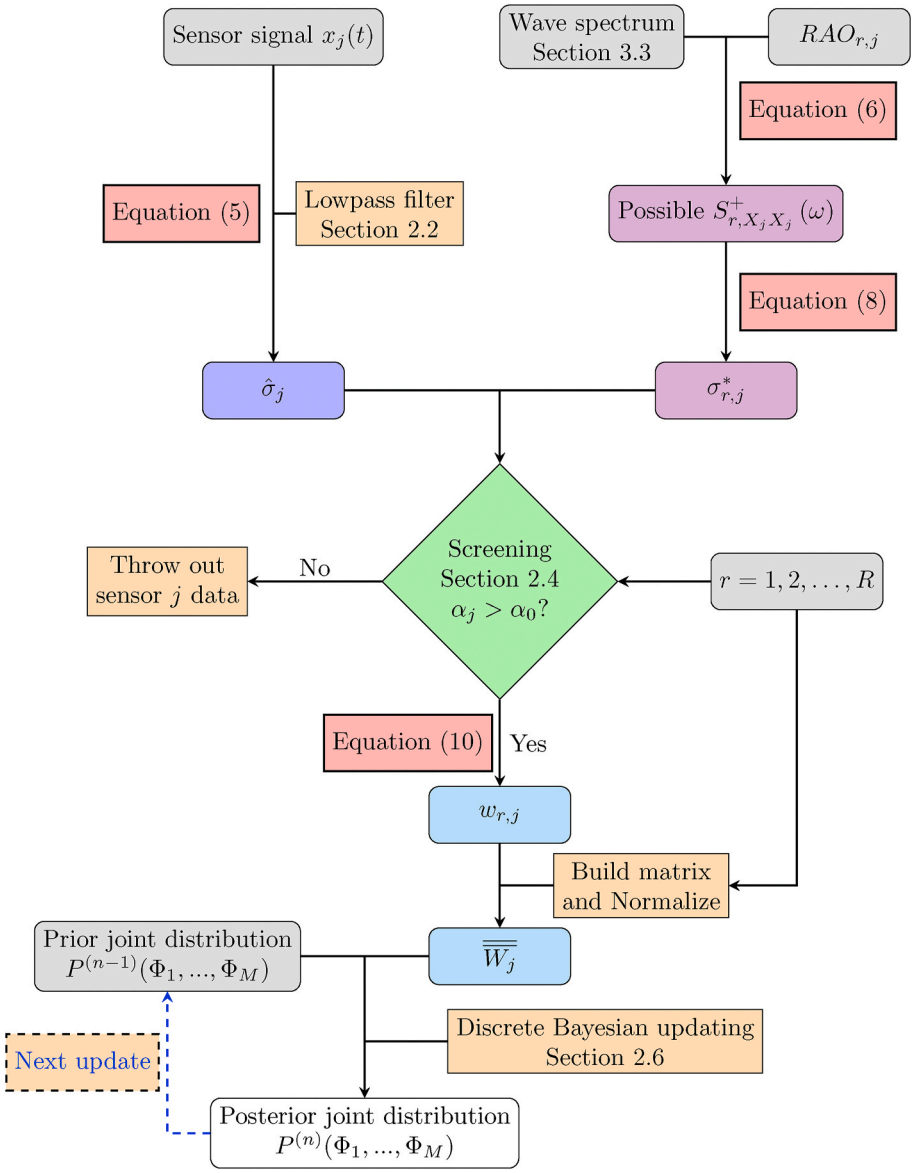

Fig. 1. Process of tuning vessel hydrodynamic model parameters, based on vessel response sensor signal.

2015). Challenges on roll motion prediction based on the vessel being modelled as a linear transfer function, known as response amplitude operator (RAO), have been reported in all the relevant tests.

A successful wave-induced vessel motion prediction requires two sources, i.e., a sufficiently accurate wave forecast and a numerical vessel model which describes the relationship between wave and vessel motion for the current operational condition. Most developed ODSS's focus on improving wave prediction, either by wave radar systems, or by the "ship as a wave buoy" analogy. Those approaches are all influenced by the vessel motion. The wave radar approaches could possibly predict the encounter waves a few minutes ahead based on a linear wave propagation model, and hence a vessel response envelope can be well estimated. However, the predicted time series of the encounter waves at the vessel position will not be accurate enough. On the other hand, nonlinear wave propagation models could better forecast the encounter waves at the vessel position, but the computational time is a challenge for real-time application (Alford et al., 2015; Grilli et al., 2011). The "ship as a wave buoy" analogy, estimating waves in the form of wave spectrum, requires good prior knowledge on vessel conditions (Nielsen, 2006; Brodtkorb et al., 2018a; Nielsen et al., 2019; Ren et al., 2021). Nielsen (2007) and Tannuri et al. (2003) demonstrated the influence of vessel condition uncertainty on the sea state estimation. Most sea state estimation approaches presume stationary environmental and vessel conditions. Iseki (2009) and (Brodtkorb et al., 2018b) investigated the influence of using non-stationary ship motion data on sea state estimation. In addition, with developed information technology, numerical weather prediction (NWP) can be improved with increased spatial and temporal resolution. Instead of only reporting the wave forecast in terms of significant wave height (H_s), peak period (T_p), and direction (β_W), a full 2D wave spectral description now can be provided by several weather forecasters (e.g., Galvin (2014)). This may also help reducing uncertainties of vessel motion prediction.

Simplifications in vessel seakeeping models have to be made in order to design the ODSS's for real-time purposes. Most ODSS's use linear transfer functions (i.e., RAOs) between wave and vessel response. Application of vessel motion RAOs has proven to be reliable, computationally cheap and practically accurate for moderate seas. Some advanced programs use retardation functions based on the hydrodynamic coefficient database to predict real-time motion in the time domain, e.g., Milewski et al. (2015). The interest of using machine learning for vessel motion analysis has increased in recent years, e.g., Cheng et al. (2019); De Masi et al. (2011); Nielsen et al. (2018). Pure

data driven and so-called physical based data-driven machine learning methods are hot research topics within several disciplines related to digitalization. The Artificial intelligence (AI) models trained by available data, are however very sensitive to the provided historical data. For nonlinear systems, the AI models may therefore fail if the training data set is insufficient with respect to describing the nonlinearity. For vessels with frequently changing loading conditions, it may be challenging to obtain sufficient training data and to generalize. AI approaches have also faced difficulties of being accepted by energy and maritime industries due to lack of physics reasoning and documented reliability.

Traditionally, hydrodynamic coefficients are calibrated to scale experiments (van Daalen et al., 2014), for predefined vessel loading conditions where the uncertainties from vessel inertia distribution and viscous roll damping could be significant. The situation onboard may be different from the designed or simulated conditions, e.g. due to the vessel having a different load condition than that originally assumed. Consequently, the presumed RAOs may not be appropriate to apply for onboard vessel motion prediction. However, improving the accuracy of RAOs based on vessel motion and wave information (e.g., H_s, T_p, β_W, and directional spreading) is practically very challenging. Normally vessel motion (e.g., heave motion η_{33}) can be estimated (Faltinsen, 1990) by

$$\eta_{33}(\omega) = \sum_{\beta_W} \zeta(\omega, \beta_W) \cdot H_{33}(\omega, \beta_W) \tag{1}$$

where $\eta_{33}(\omega)$ is the heave motion at frequency ω, $\zeta(\omega, \beta_W)$ is the wave elevation at frequency ω along the direction β_W, and $H_{33}(\omega, \beta_W)$ is the corresponding heave motion RAO. Calculating the RAO $H_{33}(\omega, \beta_W)$ represents the inverted problem of vessel motion estimation. There is typically no unique solution for such inversion problems, because $H_{33}(\omega, \beta_W)$ is direction dependent, while $\eta_{33}(\omega)$ carries no such information. Alford et al. (2014) tried to solve the inversion problem using singular value decomposition (SVD) technique to solve the ill-conditioned equation $H_{yx}(\omega) = \frac{S_{yx}(\omega)}{S_{xx}(\omega)}$. As a consequence, the directional dependency characteristics of the true transfer function will be sacrificed, making it questionable whether the calculated transfer function can be applied to a new sea state.

Instead, this paper tries to improve the RAO accuracy by modifying the important parameters in vessel seakeeping model based on wave information and vessel motion measurements. Based upon an updated hydrodynamic model, the RAO can be recalculated and possibly applied to other sea states, potentially increasing the accuracy of seakeeping prediction and the safety of marine operations. However, there are some challenges: 1) It is a multi-dimensional problem. There could be hundreds of parameters subject to uncertainty. 2) It is a multi-modal problem. Many combinations of parameters can possibly fit perfectly with the measurement data, e.g. in terms of response power spectrum, but those combinations may be far away from each other. 3) It is a nonlinear problem with respect to the relationship between hydrodynamic parameters and the resulting vessel motion RAO. In this paper, a probabilistic approach of vessel hydrodynamic parameter tuning based on onboard motion measurements is proposed, where the adaptive model will both update the parameter values and their confidence, quantitatively. This is an important step towards reliability-based marine operations and reducing inherent conservatism. The adaptive model can be continuously applied throughout the whole lifetime of the vessel, assisting in monitoring, inspection, management, life extension, etc., in accordance with the digital twin concept.

The paper is organized as follows. Section 2 details the proposed model tuning algorithm. Then the algorithm is demonstrated by case studies of a selected vessel model. The inputs and basis of the case studies are described in Section 3. Results of two studied cases are described in Section 4. Results of sensitivity analyses for key parameters in the proposed method are reported in Section 5. The proposed tuning methodology is validated by extensively simulated tuning analyses in Section 6. Conclusions and future work are then summarized in Section 7.

2. Model tuning procedure

Assume that there are M uncertain vessel parameters $(\Phi_1, \Phi_2, \ldots, \Phi_M)$ and there are J sensors measuring interesting vessel motions (e.g., displacement, velocity, and acceleration of heave and roll at different locations onboard). Based on the prior knowledge on the uncertain vessel parameters and available vessel sensors $j = 1, 2, \ldots, J$, a RAO database covering all possible vessel conditions for all sensors should be available for the tuning process. The procedure for tuning of vessel parameters $(\Phi_1, \Phi_2, \ldots, \Phi_M)$ based on measurements from onboard sensors at a specific sea state can be divided into the following steps as illustrated in Fig. 1:

1. Initialize the discrete joint probability distribution $P^{(0)}(\Phi_1, \Phi_2, \ldots, \Phi_M)$ based on prior knowledge on the vessel condition.
2. Process the sensor measurements (e.g., signal $x_j(t)$ from sensor j), including signal filtering and calculation of the filtered signal standard deviation $\widehat{\sigma}_j$.
3. Calculate the standard deviations of the possible responses $\sigma^*_{r,j}$, based on the candidate RAOs from the RAO database. $r \in \{1, 2, \ldots, R\}$ represents the r^{th} combination of variables in the RAO database, i.e., $(\Phi_{i1}, \Phi_{i2}, \ldots, \Phi_{im}, \ldots, \Phi_{iM})$, where Φ_{im} the im^{th} discrete value for the vessel parameter Φ_m and $m \in \{1, 2, \ldots, M\}$. R is the total number of possible combinations of uncertain vessel parameters.
4. Screen out less significant sensors.
5. Calculate the weight matrix $\overline{\overline{W_j}}$ for the considered whole range of uncertain vessel parameters, if sensor j passes the above screening phase.
6. Normalize $\overline{\overline{W_j}}$, and interpolate the weight matrix $\overline{\overline{W_j}}$ from the size $I1 \times I2 \times \cdots \times IM$ (variable resolution in the RAO database) to the size $K1 \times K2 \times \cdots \times KM$ (variable resolution in the discrete probability distribution model).
7. Update the joint probability distribution $P^{(1)}(\Phi_1, \Phi_2, \ldots, \Phi_M)$.
8. Repeat the previous steps, and continuously update the variable distribution, $P^{(2)}(\Phi_1, \ldots, \Phi_M)$, …, $P^{(n)}(\Phi_1, \ldots, \Phi_M)$, ….

All steps are explained in the following subsections. The detailed parameter explanations can be found in Nomenclature.

2.1. Initialization of joint probability distribution

The probabilistic model of the M uncertain vessel parameters can be initialized as independent Gaussian distributions with presumed mean μ_m and variance σ_m^2 for each variable, based on prior knowledge on the vessel.

$$\Phi_m \sim Gaussian(\mu_m, \sigma_m^2) \tag{2}$$

The variance of each variable depends on vessel geometry, loading condition, engineering judgement and etc. It is further assumed that the possible values of the variable Φ_m are within the range of $\mu_m \pm 3\sigma_m$. In the joint probability distribution model, each variable was discretized into Km number of values. A multivariate probabilistic model with M uncertain variables can be expressed by a discrete joint probability distribution $P(\Phi_1, \Phi_2, \ldots, \Phi_M)$. The probability density function of one possible combination of $(\Phi_1, \Phi_2, \ldots, \Phi_M)$ is expressed by $PDF(\Phi_{k1}, \Phi_{k2}, \ldots, \Phi_{kM})$, which is established by

$$PDF(\Phi_{k1}, \Phi_{k2}, \ldots, \Phi_{kM}) = \prod_{m=1}^{M} PDF(\Phi_{km}) \tag{3}$$

The probability for this combination can then be calculated by

$$P(\Phi_{k1}, \Phi_{k2}, \ldots, \Phi_{kM}) = PDF(\Phi_{k1}, \Phi_{k2}, \ldots, \Phi_{kM}) \cdot \prod_{m=1}^{M} \Delta\Phi_m \tag{4}$$

where $\Delta\Phi_m$ means the interval of values for the variable Φ_m. Unrealistic values such as negative values for damping were removed in the initialization step for probabilistic modelling. In addition, normalization of the probability distribution was done through every tuning step. This was to ensure that the cumulative probability sums to 1.0.

2.2. Signal processing

Sensitivity analysis with respect to signal lowpass filtering demonstrated that it is essential to filter out noise before the probability updating process. The fast Fourier transform (FFT) lowpass filtering approach was applied with 1.0 Hz as the cutoff frequency (f_{lp}) for the base case in the case studies. The filtered signal for sensor j is denoted as $\widehat{x}_j(t)$. After filtering, the signal standard deviation can be calculated by means of the unbiased sample standard deviation:

$$\widehat{\sigma}_j = \sqrt{\frac{\sum_{t=1}^{N_t}\left(\widehat{x}_j(t) - \overline{x}_j\right)^2}{(N_t - 1)}} \tag{5a}$$

$$\overline{x}_j = \frac{\sum_{t=1}^{N_t}\widehat{x}_j(t)}{N_t} \tag{5b}$$

where $\widehat{x}_j(t)$ is the filtered vessel response time series from sensor j for the time step t and N_t is the number of time steps. The original noisy sensor signal $x_j(t)$ (in time domain) or $X_j(\omega)$ (in frequency domain) can be measurement of the vessel displacement, velocity, or acceleration for any degree of freedom (DOF).

2.3. Calculation of possible response spectra based on candidate RAOs

For a certain sensor numbered as j, within the known ranges of the uncertain vessel hydrodynamic parameters, the corresponding possible response spectra can be calculated by

$$S^{+}_{r,X_jX_j}(\omega) = \left|H_{r,X_j\zeta}(\omega,\beta_W)\right|^2 \cdot S^{+}_{\zeta\zeta}(\omega,\beta_W) \tag{6}$$

where S^{+} means single sided power spectrum, $H_{r,X_j\zeta}(\omega,\beta_W)$ represents the linear transfer function (i.e., RAO) between the interesting vessel response $X_j(\omega)$ at the sensor j and wave elevation $\zeta(\omega,\beta_W)$, for the r^{th} combination of variables in the RAO database, $r \in \{1,2,\ldots,R\}$ and

$$R = \prod_{m=1}^{M} Im \tag{7}$$

where Im is the number of discrete values for variable Φ_m in the RAO database. Then the possible response standard deviation for the r^{th} combination can be calculated by

$$\sigma^*_{r,j} = \sqrt{\sum_{n=1}^{N_\omega} S^{+}_{r,X_jX_j}(\omega_n)\cdot\Delta\omega} \tag{8}$$

where N_ω is the total number of discretized frequencies for the response spectrum.

2.4. Screening of sensors

If the variation of the considered parameters influences the sensor j measurements very little, all calculated $\sigma^*_{r,j}$ values will be very close. Then this sensor should be considered as valueless, based on the following arguments:

1. The other uncertainties from e.g., simplification of vessel hydrodynamics, measurement noise, discretization of signals and power spectra, and wave hindcast, will be much more significant than the present parameter variations. Under such condition, updating parameters becomes unreasonable.
2. For the weight calculation to be described in Section 2.5, if $\left|\sigma^*_{r,j} - \widehat{\sigma}_j\right| \to 0$, the weight $w_{r,j}$ could be very large. A small amount of noise or other uncertainties may result in a significantly biased weight matrix.

Therefore, it is important to identify and ignore valueless sensors for each sea state before updating the joint probability distribution of the uncertain vessel parameters. Consequently, a new parameter α_j is introduced, named SSR (sensor screening ratio) which is defined by

$$\alpha_j = \frac{\sigma_{\sigma^*_{r,j}}}{\widehat{\sigma}_j} \tag{9a}$$

$$\sigma_{\sigma^*_{r,j}} = \sqrt{\frac{\sum_{r=1}^{R}\left(\sigma^*_{r,j} - \overline{\sigma^*_j}\right)^2}{R-1}} \tag{9b}$$

$$\overline{\sigma^*_j} = \frac{\sum_{r=1}^{R}\sigma^*_{r,j}}{R} \tag{9c}$$

where $\sigma_{\sigma^*_{r,j}}$ is the standard deviation of $\sigma^*_{r,j}$, $r = 1,2,\ldots,R$. The base case studies used a screening criterion of $\alpha_j = 0.05$. For a certain sensor j, if $\alpha_j < 0.05$, then the sensor j will be excluded when updating the parameters. Selection of the α_j value may depend on the quantity and location of the sensor, the sea state, and the selected vessel parameters to be modified.

2.5. Weight calculation

The distance between $\sigma^*_{r,j}$ and $\widehat{\sigma}_j$ represents how much the r^{th} combination of the parameters can be believed in based on the received measurements at sensor j. The weight factor can be calculated by inverse distance weighting introduced by Shepard (1968). Normalization is applied to the weight matrix before updating the joint probability distribution of parameters.

$$w_{r,j} = \left\| \frac{1}{\left|\sigma^*_{r,j} - \widehat{\sigma}_j\right|^p} \right\| \tag{10}$$

where $p \in (0,\infty)$ is called the power parameter and $\|\cdot\|$ is a normalization operator.

2.6. Discrete Bayesian updating

Classical discrete Bayes' theorem may be simply expressed as

$$P(U|V) = \frac{P(U)\cdot P(V|U)}{P(V)} \tag{11}$$

where U and V are events. $P(U|V)$ is the likelihood of event U occurring given that V is true while $P(V|U)$ is the likelihood of event V occurring given that U is true. For the tuning of vessel hydrodynamic parameters, U can be considered as those uncertain parameters, while V corresponds to the received sensor signals. However, the Bayesian inference may not seem so simple as shown in Equation (11), due to the practical difficulties of estimating $P(V|U)$ and $P(V)$. Inspired by Labbe (2018), the Bayesian updating applied for model tuning could also be understood as:

$$posterior = \frac{prior\cdot likelihood}{normalization} \tag{12}$$

where *likelihood* means the possibility of getting such measurement (e.g., sensor j) result for the particular combination (e.g., r) of uncertain vessel

Table 1
Vessel information, base case.

Parameters	Description	Value	Unit
L_{PP}	Length between perpendiculars	~120	m
B	Breadth	~27	m
D (Ballast)	Draft	~5.1	m

parameters, which can be reasonably represented by the weight factor $w_{r,j}$. This is the key to updating our belief to the prior knowledge after receiving the sensor data. With Equation (10), $w_{r,j}$ is calculated based on the discrete vessel parameter values used in the RAO database. For one sensor j, the size of the calculated weight matrix $\overline{\overline{W_j}}$ for M variables by Equation (10) is $I1 \times I2 \times \cdots \times IM$. However, the joint probability distribution of variables uses much more discrete values than was used to build RAO database. In order to update the joint distribution of variables, the weight matrix needs to be interpolated to the size of $K1 \times K2 \times \cdots \times KM$. Multi-dimensional linear interpolation was performed by means of the Python xarray package (Hoyer and Hamman, 2017).

Discrete Bayesian updating could easily apply to nonlinear systems such as the described hydrodynamic parameter tuning challenge. Due to the nonlinearity, the updated probability distribution will have no closed-form mathematical description after the first update, and the updated probability distribution will no longer be Gaussian. The n^{th} updating for the r^{th} combination of uncertain vessel parameters based on the valuable sensor j data can then be formulated as:

$$PDF^{(n)}(\Phi_{k1}, \ldots, \Phi_{kM}) = PDF^{(n-1)}(\Phi_{k1}, \ldots, \Phi_{kM}) \cdot w_{r,j} \tag{13}$$

3. Case study basis

3.1. Numerical vessel model

The case study was based on an offshore supply vessel (OSV) hydrodynamic seakeeping model. The primary vessel dimensions are summarized in Table 1. The coordinates refer to the reference coordinate system moving steadily at the vessel forward speed, as illustrated in Fig. 2. The positive x-axis points from stern to bow ($x = 0$ aft), the z-axis is pointing vertically upward from keel ($z = 0$ at keel) and the y-axis is normal to the $x - z$ plane where $y = 0$ is at the longitudinal symmetric plane. The wave direction β_W follows the same coordinate system, i.e. waves at 0° heading propagates along the positive x-axis. Table 2 summarizes the location and ID of the virtual sensors considered in the paper. The sensor locations are illustrated in Fig. 2. Practically, the vessel heave response could dominate the operation limit, and hence it is usually of interest to monitor the heave response. Earlier parametric sensitivity study (Han et al., 2020) suggests that measuring different quantities of vessel response (i.e., displacement, velocity, and acceleration) at different locations onboard can help identifying the right uncertain parameter to tune. Therefore, the RAO database contains the heave response (displacement, velocity and acceleration), at three different locations, see Fig. 2. Rigid body motion transformation was assumed in the study.

3.2. RAO database

A RAO database was established based on the ballast condition as the base case. Wasim (DNV GL, 2018) was used for hydrodynamic analysis to create the RAO database. Being a computer program in the DNV GL Sesam family, Wasim is a 3D time-domain hydrodynamic analysis software based on the Rankine panel method (Kring, 1994). Wasim analyses were run through all wave periods for each combination of the studied parameters in the time domain. The outputs were transferred to the frequency domain so as to build the frequency dependent database of hydrodynamic coefficients and thereafter calculate the vessel RAOs by

Table 2
Description of sensor measurements.

Sensor ID	Location	Coordinate (x,y,z) [m]	Signal/measurements
Disp_A	A	(60.0, 0.0, 10.0)	$\eta_{33}(t)$ at location A
Disp_B	B	(60.0, 13.0, 10.0)	$\eta_{33}(t)$ at location B
Disp_C	C	(0.0, 10.0, 14.0)	$\eta_{33}(t)$ at location C
Vel_A	A	(60.0, 0.0, 10.0)	$\dot{\eta}_{33}(t)$ at location A
Vel_B	B	(60.0, 13.0, 10.0)	$\dot{\eta}_{33}(t)$ at location B
Vel_C	C	(0.0, 10.0, 14.0)	$\dot{\eta}_{33}(t)$ at location C
Acc_A	A	(60.0, 0.0, 10.0)	$\ddot{\eta}_{33}(t)$ at location A
Acc_B	B	(60.0, 13.0, 10.0)	$\ddot{\eta}_{33}(t)$ at location B
Acc_C	C	(0.0, 10.0, 14.0)	$\ddot{\eta}_{33}(t)$ at location C

$\eta_{33}(t)$: time series of heave displacement; $\dot{\eta}_{33}(t)$: time series of heave velocity; $\ddot{\eta}_{33}(t)$: time series of heave acceleration.

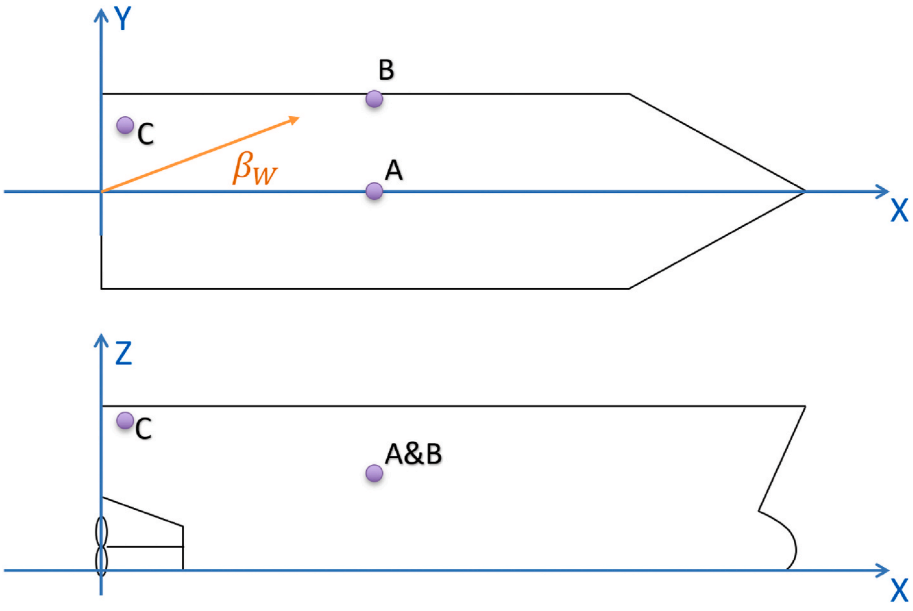

Fig. 2. Illustration of vessel coordinate system and locations of considered interesting points.

Table 3
Parametric range for the considered variables.

Parameters	Variation range	Number of values
Mass	[-6%, +6%]	7
XCG	[-4 m, +4 m]	5
r_{55}	[-9%, +9%]	7
GMT[a]	[0, 1 m]	6
β_{44}	[2%, 14%]	7

[a] Here "GMT" represents the free surface correction to the transverse metacentric height. $GMT = 0.5$m here means that the transverse metacentric height is corrected with -0.5m due to free surface effects. It is not the value of the transverse metacentric height.

$$RAO(\omega, u|\beta_W) = \frac{\overrightarrow{F}(\omega, u|\beta_W)}{-\omega_e^2\left(\overline{\overline{A}}(\omega_e) + \overline{\overline{M_0}}\right) + i\omega_e\overline{\overline{\beta}}(\omega_e) + \overline{\overline{C}}} \tag{14}$$

where ω is the wave frequency, u is the vessel advancing speed, and β_W is the wave heading as illustrated in Fig. 2. $\overrightarrow{F}(\omega, u|\beta_W)$ is the complex-valued wave-induced excitation force, and ω_e is the encounter frequency. $\overline{\overline{A}}$, $\overline{\overline{M_0}}$, $\overline{\overline{\beta}}$ and $\overline{\overline{C}}$ are the added mass matrix, inertia matrix, damping matrix and restoring stiffness matrix of the vessel, respectively.

Only heave RAOs corresponding to the sensors described in Table 2 were included in the RAO database. As summarized in Table 3, variation of 5 parameters were considered for the RAO database, with the described number of discrete values for each parameter. Selection of parameters was based on sensitivity studies of hydrodynamic parameters that influence the vessel motions of interest. Some key findings on the parametric sensitivity study (Han et al., 2020) are: 1) GMT and additional roll damping (β_{44}) both have a strong influence on the roll motion response; 2) Parameters related to the inertia distribution such as XCG, YCG, ZCG, mass and r_{55} have a strong influence on the vessel heave motion at different locations onboard, among which XCG and r_{55} are the most important parameters; 3) YCG only has significant influence on the vessel roll motion and its coupled motions. The ranges represent prior knowledge and the corresponding uncertainties for the parameters. Zero vessel speed was considered in order to avoid dealing with the 3-to-1 mapping problem between wave frequency and encounter frequency for following waves (Nielsen, 2017). In total, 13 wave headings between 0° and 180° with 15° interval were included. Therefore, each sensor in Table 2 has hundreds of thousands heave RAOs prepared.

3.3. Wave spectrum

Ocean waves are usually short-crested in reality. In addition, a sea state may contain both wind sea and swells coming from totally different main directions with significantly distinct peak periods. Precise knowledge on the wave condition was assumed for the studied cases, i.e. uncertainties from wave hindcast/forecast were not considered. For simplicity, the long-crested Pierson-Moskowitz (PM) spectrum $S_{PM}(\omega)$ was used (DNVGL-RP-C205, 2017).

$$S_{PM}(\omega) = 5 \Big/ 16 \cdot H_s^2\omega_p^2\omega^{-5} exp\left(-5 \Big/ 4\left(\frac{\omega}{\omega_p}\right)^{-4}\right) \tag{15}$$

where H_s is the significant wave height, and ω_p is the sea state peak frequency.

3.4. Sensor signal simulation

Virtual sensor signals were numerically simulated for the case studies. For each of the 9 virtual sensors described in Table 2, the signals were generated, according to the procedure illustrated in Fig. 3. Firstly, with known wave spectrum $S_{\zeta\zeta}^+(\omega, \beta_W)$ and the true RAO values for

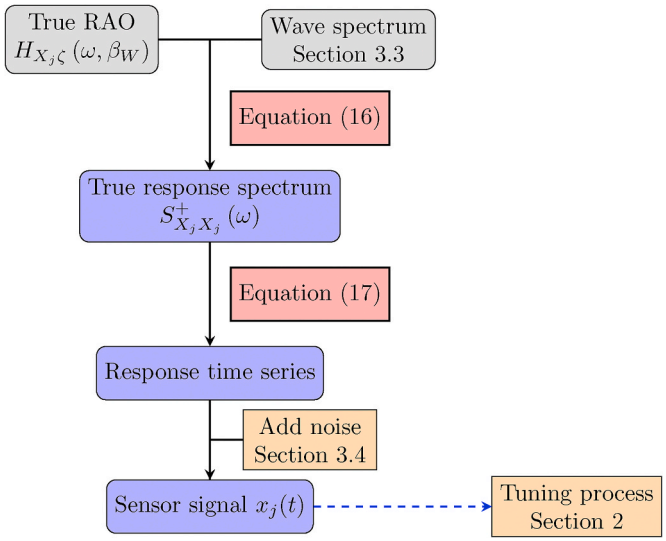

Fig. 3. Process of generating virtual sensor signal $x_j(t)$ for sensor j.

sensor j, the response spectrum can be calculated by

$$S_{X_jX_j}^+(\omega) = \left|H_{X_j\zeta}(\omega, \beta_W)\right|^2 \cdot S_{\zeta\zeta}^+(\omega, \beta_W) \tag{16}$$

where $H_{X_j\zeta}(\omega, \beta_W)$ represents the true RAO for vessel response $X_j(\omega)$. Then the signal of 3-hour response time series with time step of 0.1s was generated by

$$x_j(t) = \sum_{n=1}^{N\omega} N_\omega C_n(\omega_n)\cos(\omega_n t + \phi_n) \tag{17a}$$

$$C_n(\omega_n) = \sqrt{2S_{X_jX_j}^+(\omega_n)\cdot\Delta\omega} \tag{17b}$$

where $\phi_n \in [0, 2\pi)$ is a random phase angle which is continuous and uniformly distributed, $\Delta\omega$ is the width of the radial frequency interval of ω_n, and N_ω is the total number of the discrete frequencies for the response spectrum. Deterministic amplitudes were applied according to Equation (17b). This means that theoretically all possible realizations will return exactly the same response power spectrum when $\Delta\omega \to 0$.

Sensor signal noises were included. Gaussian distributed white noise was assumed with mean value $\mu_N = 0$ and a specified covariance σ_N^2. The noise was added to each time step of the time series independently, according to the specified signal-to-noise Ratio (SNR), defined by

$$SNR = \frac{\sigma_X^2}{\sigma_N^2} \tag{18}$$

where, σ_X^2 is the variance of the true response time series.

However, note that in reality, the sensor noise may be biased and non-Gaussian distributed (Labbe, 2018). Practically, the velocity can be calculated by integration of acceleration time series, while the displacement can be calculated by another integration over the velocity time series. The noise associated with displacement, velocity and acceleration signals are therefore correlated. However, this correlation is currently not considered. The noises of acceleration, velocity and displacement time series were added independently.

4. Case study results

Case studies were conducted to test the proposed methodology. For illustration purposes, each case only includes two parameters to tune. The sea states in Table 4 were applied. The key parameters used in the tuning process are summarized in Table 5.

Table 4
Sea states for the case studies.

Sea state ID	H_s [m]	T_z [s]	β_W [°]	Seed number
SS1	2.0	6.0	90	11
SS2	4.0	10.0	30	27
SS3	3.0	7.0	45	52
SS4	1.5	4.0	60	19
SS5	2.5	8.5	105	43

Table 5
Key parameters of tuning approach in the base case studies.

Parameters	Value	Unit
SNR (Equation (18))	100	–
α_j (Equation (9a))	0.05	–
p (Equation (10))	0.3	–

Table 6
Prior information and true values of GMT and β_{44}.

Parameter	Mean	σ^2	$\pm 3\sigma$	True value
GMT [m]	0.5	0.015	[0.13, 0.87]	0.40
β_{44} [-]	0.07	4.00E-04	[0.01, 0.13]	0.04

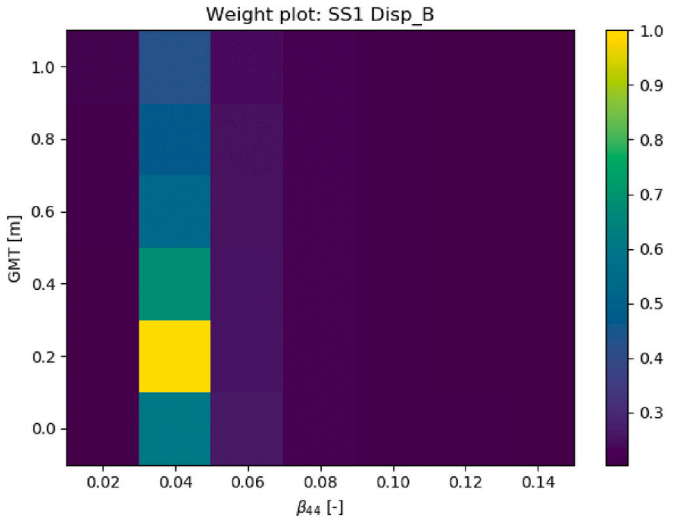

Fig. 4. Example of weight matrix, based on Disp_B sensor measurement for SS1.

4.1. GMT and β_{44}

The first case study considered GMT and β_{44} as the uncertain vessel hydrodynamic parameters. The other three parameters (i.e., XCG, mass and r_{55}) were set as deterministic. The prior knowledge and the true values of GMT and β_{44} are summarized in Table 6.

The calculated weight matrix illustrated in Fig. 4, indicates that the considered parameters GMT and β_{44} are sensitive to the Disp_B sensor for the SS1 sea state. It is obvious that GMT and β_{44} influence the roll motion very much, and SS1 is a beam sea condition with the peak period approximately near the heave RAO peak amplitude period for the location B. On the other hand, Fig. 5 illustrates a confusing weight matrix. The weight factor is spreading over a large variable range, because the sea state SS4 is with $T_z = 4.0$ s ($T_p = 5.6$ s). There was barely no significant vessel response around that small response period due to the lowpass filtering nature of the vessel. This means that GMT and β_{44} do not have significant influence on the RAOs and vessel motion for the

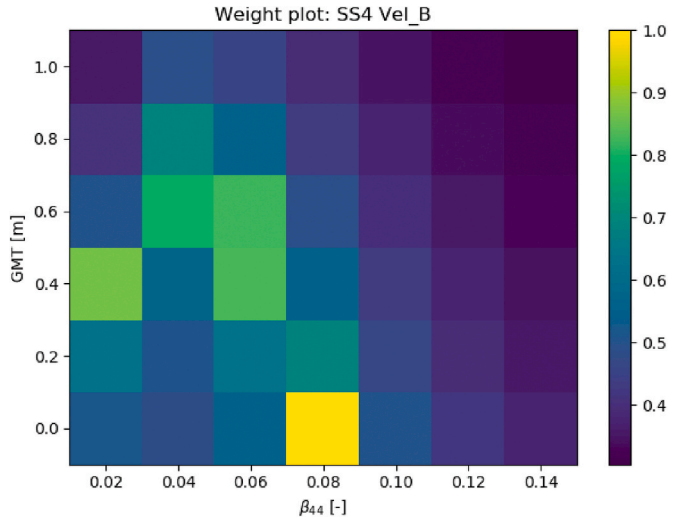

Fig. 5. Example of weight matrix, based on Vel_B sensor measurement for SS4.

Table 7
Intermediate tuning results - *GMT* [m] and β_{44}.

Sea state	μ_{GMT}	σ^2_{GMT}	$\mu_{\beta_{44}}$	$\sigma^2_{\beta_{44}}$	Number of valuable sensors
Initial	0.5	0.0145[a]	0.07	3.86E-04[a]	N/A
SS1	0.34	0.0145	0.042	4.61E-05	6
SS2	0.31	0.0112	0.041	1.97E-05	2
SS3	0.33	0.0125	0.041	1.08E-05	3
SS4	0.38	0.0180	0.041	1.17E-05	2
SS5	0.35	0.0128	0.041	5.85E-06	6

[a] It is different from the initial variance summarized in Table 6, due to a normalization procedure during initialization described in Section 2.1.

given sea state SS4. The variance of GMT and β_{44} were increased after tuning based on SS4, as shown in Table 7, meaning that the tuning system got confused by the sensor data for SS4. Both parameters do not influence the heave motion at the COG and therefore, the measurements at the location A near the COG were screened out for all tuning steps.

Fig. 6 illustrates the tuning results based on response measurements from each sea state. SS1 and SS5 played important roles with respect to the successful tuning, while SS4 attempted to degrade the tuning results. It is noted that sensor data from SS1 over-tuned the probability distribution of GMT, due to signal noises. This problem is discussed in detail in Section 5.4 and Section 5.5.

4.2. XCG and mass

The same sea states defined in Table 4 were applied for tuning the XCG and the mass, however, with a different vessel condition. The prior knowledge and the true values of XCG and mass are summarized in Table 8.

The results in Fig. 7 and Table 10 show that SS3 and SS4 significantly contributed to the tuning of XCG in the correct direction. Both sea states are oblique waves with small wave periods, where the hydrodynamic parametric sensitivity studies (Han et al., 2020) showed that the vessel heave motion are sensitive to XCG. As illustrated in Fig. 7, the joint probability distribution was not updated from SS5, meaning that all sensor measurements from SS5 were screened out. In other words, XCG and mass have negligible effects to the considered vessel response at SS5. The weight matrix examples shown in Fig. 8 indicate the system "confusion". All the 4 sensor measurements successfully gave high weight to the correct XCG value, but failed with respect to tuning vessel mass. The measurements from sensor Acc_B gave approximately the same weight factor through the whole range of mass values.

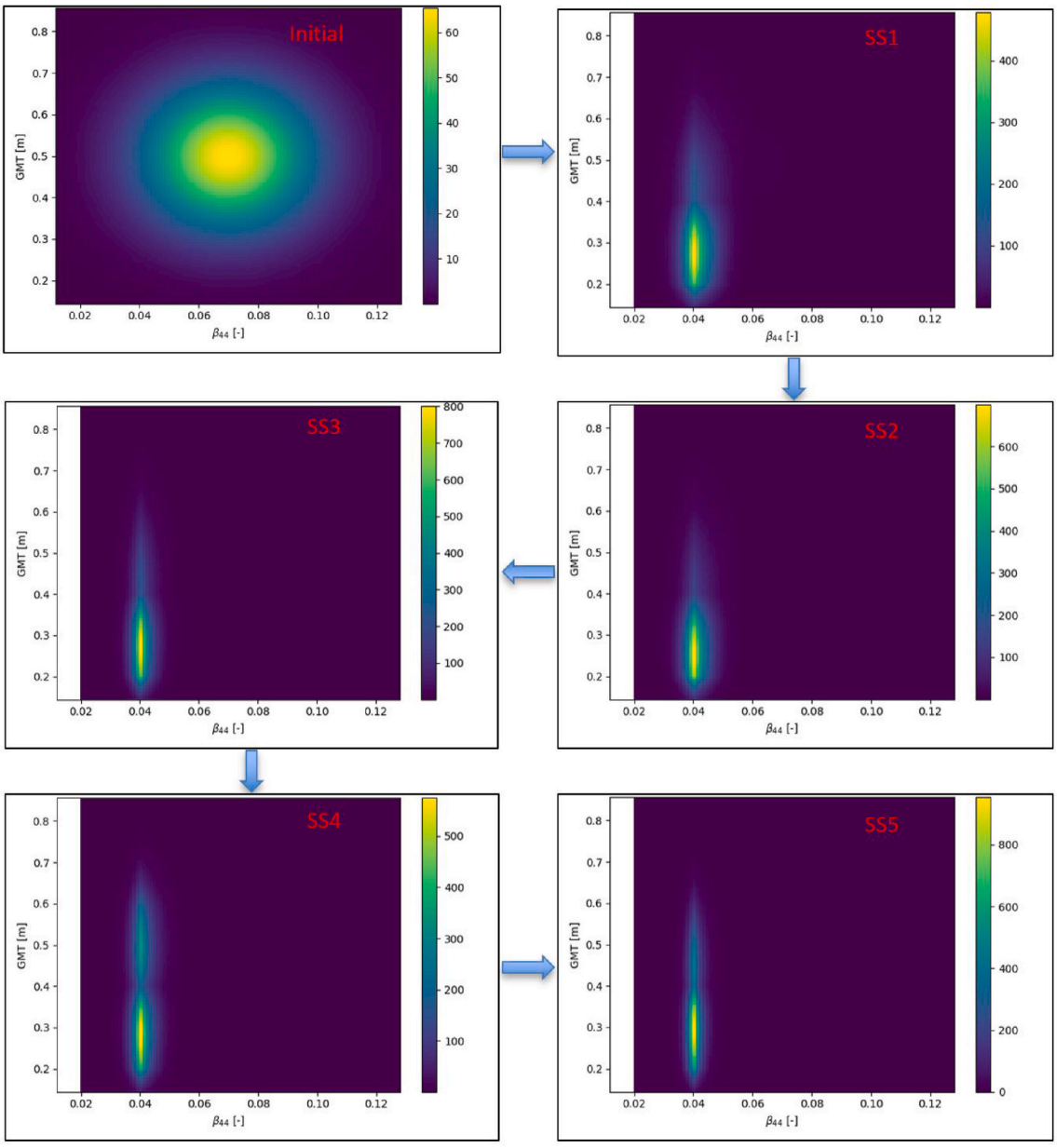

Fig. 6. Intermediate tuning results of the joint probability distribution of GMT and β_{44} from measurements for each sea state.

Table 8
Prior information and true values of XCG and Mass.

Parameter	Mean	σ^2	$\pm 3\sigma$	True value
XCG [m]	59.4	1.21	[56.23, 62.56]	57.4
Mass [t]	12,166.5	59,000	[11,467, 12,865]	11,680

Measurements from Disp_C and Vel_B sensors gave almost the opposite weighting distribution along mass values. The parametric sensitivity study (Han et al., 2020) showed that vessel mass influences the heave velocity mostly at small response periods for head and following sea conditions. At the given uncertainty ranges, the mass variation is less important with respect to the vessel response compared with XCG. Therefore, it is not very surprising that the measurements from the selected sea states failed to tune the vessel mass, due to 1) its less sensitivity for the considered sea states; 2) the nonlinear nature of the vessel response to the hydrodynamic parameters; 3) the measurement noise and uncertainties by e.g., seed variation. Therefore, measurements from one more sea state (SS6 in Table 9) were provided. SS6 was expected to be relatively sensitive with respect to the mass coefficient. Fig. 9 shows a dramatic shift of the peak of the joint distribution to a lower mass value.

5. Parametric sensitivity study

The case study of tuning GMT and β_{44} presented in Section 4.1 was chosen as the base case for the sensitivity study of some key parameters in the tuning algorithm.

5.1. Power parameter p

$p = 0.1, 0.5$ and 1.0 were chosen as the sensitivity study cases. The tuning results are summarized in Table 11. As shown in Fig. 10, large p leads to very large weight factor, which could be risky especially when $\left|\sigma^*_{r,j} - \hat{\sigma}_j\right| \to 0$. Therefore large p may lead to quick and abrupt change of

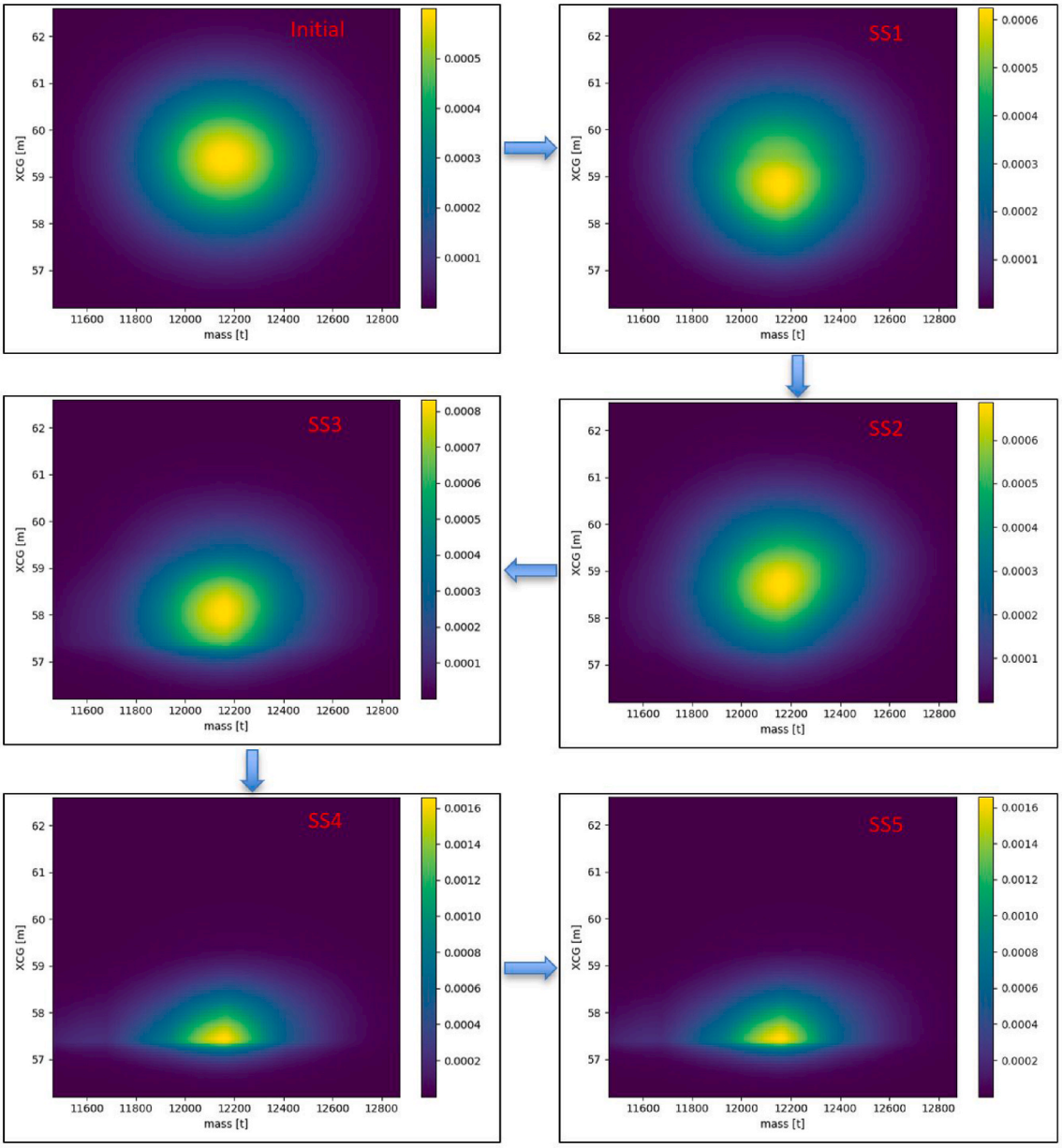

Fig. 7. Intermediate tuning results of the joint probability distribution of XCG and mass from measurements for each sea state.

Table 9
Additional sea state for model tuning of mass coefficient.

Sea state ID	H_s [m]	T_z [s]	β_W [°]	Seed number
SS6	1.5	5.5	15	8

the joint probability distribution of parameters, as illustrated in Fig. 11. Larger p value leads to less "memory" of the tuning results from the previous sea states. This may not be practically reasonable, especially for a stationary vessel situation, due to the existing uncertainties. The vessel loading condition could be considered as stationary for a relatively long time, e.g., in terms of days. If the focus is only to tune the sea state dependent parameters, e.g., β_{44}, larger p value might be preferable. But cautions are required to use large p for tuning multiple parameters at the same time.

Table 10
Intermediate tuning results - XCG [m] and mass [t].

Sea state	μ_{XCG}	σ^2_{XCG}	μ_{mass}	σ^2_{mass}	Number of **valuable sensors**
Initial	59.4	1.17[a]	12,166	56,969[a]	N/A
SS1	59.1	1.2	12,153	54,231	1
SS2	58.9	1.01	12,154	56,177	2
SS3	58.4	0.77	12,150	57,587	3
SS4	57.8	0.33	12,145	58,806	6
SS5	57.8	0.33	12,145	58,806	0
SS6	57.6	0.18	11,910	11,4640	7

[a] It is different from the initial variance summarized in Table 8, due to the normalization procedure described in Section 2.1.

5.2. SNR

It is interesting to test the performance of the proposed tuning approach with respect to the signal noise level. The sensitivity analysis

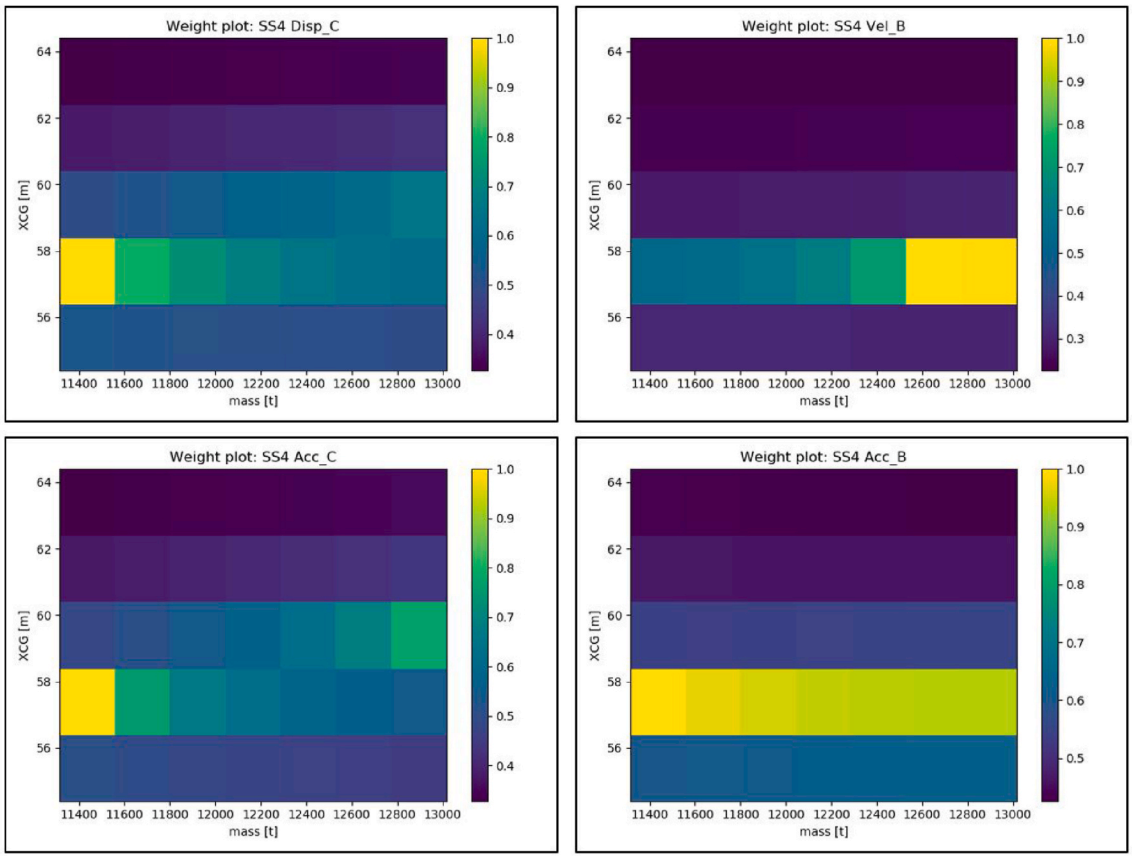

Fig. 8. Examples of weight matrix for tuning of XCG and mass from measurements for SS4.

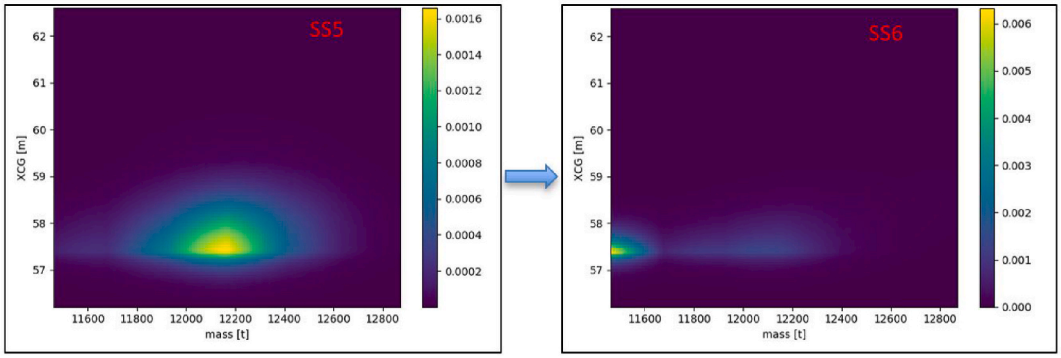

Fig. 9. Tuning results of probability distribution of XCG and mass due to measurements from SS6.

Table 11
Sensitivity with respect to power parameter.

p	μ_{GMT}	σ^2_{GMT}	GMT P90 interval[a]	$\mu_{\beta_{44}}$	$\sigma^2_{\beta_{44}}$
0.1	0.46	0.0150	[0.26, 0.66]	0.044	8.95E-05
0.3	0.35	0.0128	[0.17, 0.54]	0.041	5.85E-06
0.5	0.28	0.0057	[0.16, 0.41]	0.040	3.48E-06
1	0.26	0.0020	[0.19, 0.33]	0.040	2.70E-06

[a] 5− and 95− percentile values.

on SNR therefore also serves a purpose of validating the methodology. The lowpass filter method does not require to know the noise level explicitly. Results in Table 12 show that the methodology is quite stable with respect to dealing with signal noises. The tuning results in terms of mean and variance of the parameters are close for all SNR values varying from 10 to 10,000.

5.3. Seed variation

The seeds for generating vessel response sensor signals had been selected for all previous studies, ensuring exactly the same signals for tuning result comparison. The importance of seed variation with respect to the tuned results was investigated. Seeds were randomly generated for the same 5 sea states. In total, 10 sets of randomly generated seeds were used for the 5 sea states, corresponding to 10 tuning results, named as from Case1 to Case10. As shown in Fig. 12, the tuning results of β_{44} were very stable, in terms of its expected value and variance. This is due to very sensitive and monotonic influences from β_{44} to vessel response (i.e., RAO). The additional roll damping only influences the RAO amplitude, but not the RAO peak period. Fig. 12 shows that seed variation could significantly influence the tuning results for the parameters which

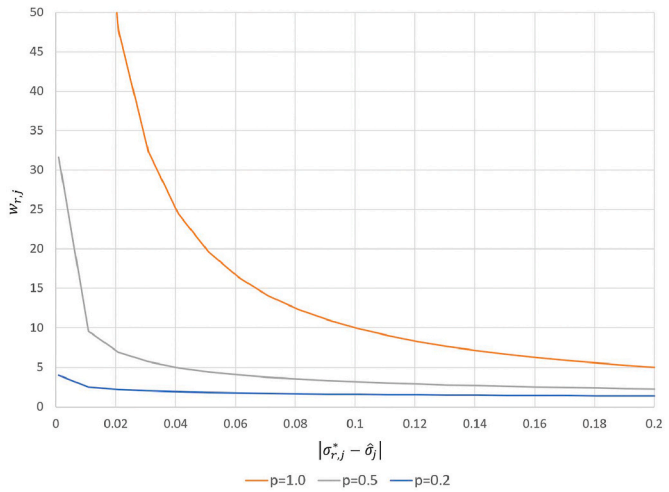

Fig. 10. Influence of power parameter on weight factor along $\left|\sigma^*_{r,j} - \hat{\sigma}_j\right|$.

are not very sensitive to the vessel response at those sea states (e.g., GMT) as variation in tuned GMT was observed. This is because 1) vessel response RAO is less sensitive to GMT; 2) the correlation between GMT and vessel RAO is complex. GMT shifts the RAO amplitude peak period, and changes the amplitude magnitude, as GMT determines the restoring stiffness for roll response. It is also noted that the variance of GMT did not reduce significantly through tuning based on measurements from the selected sea states.

5.4. Lowpass filtering cutoff frequency

Considering noise, the signal variance is equal to:

$$\sigma^2_{signal} = \sigma^2_X + \sigma^2_N \tag{19}$$

where σ^2_X and σ^2_N are the variance of the true response time series and the signal noise, respectively. Theoretically without processing signal noise, the variance of the signal will always be larger than the true response variance, potentially leading to biased tuning results. Therefore, the noise should be removed as much as possible. The noise power cannot be known exactly by nature. Section 5.2 demonstrated the robustness of applying a lowpass filter to deal with noise. A sensitivity study with respect to the cutoff frequency was carried out. The results are summarized in Table 13 for tuning GMT and β_{44}, and Table 14 for tuning XCG and mass.

Both Tables 13 and 14 show that $f_{lp} = 0.2$ Hz almost always gave the best tuned results in terms of being closer to the true values and with less variance. Exceptions were observed for the variance of the tuned vessel mass in Table 14. The mass variance σ^2_{mass} after tuning was larger than the initiated variance for all seed variations, indicating the system "confusion" mentioned in Section 4.2 due to the less sensitivity of mass on the vessel response for the considered sea states. Deep investigation of intermediate results indicated that the noise variance filtered out was actually always less than the true noise variance for the base case (i.e., $f_{lp} = 1.0$ Hz). Consequently, the variances of the filtered signal time series were all biased to a higher value than the true response. This led to biased tuning results.

Table 12
Sensitivity with respect to SNR.

SNR	μ_{GMT}	σ^2_{GMT}	GMT P90 interval[a]	$\mu_{\beta_{44}}$	$\sigma^2_{\beta_{44}}$
10	0.41	0.0182	[0.18, 0.63]	0.041	9.33E-06
100	0.35	0.0128	[0.17, 0.54]	0.041	5.85E-06
1000	0.39	0.0110	[0.22, 0.56]	0.041	5.91E-06
10,000	0.39	0.0108	[0.22, 0.56]	0.041	5.89E-06

[a] 5– and 95– percentile values.

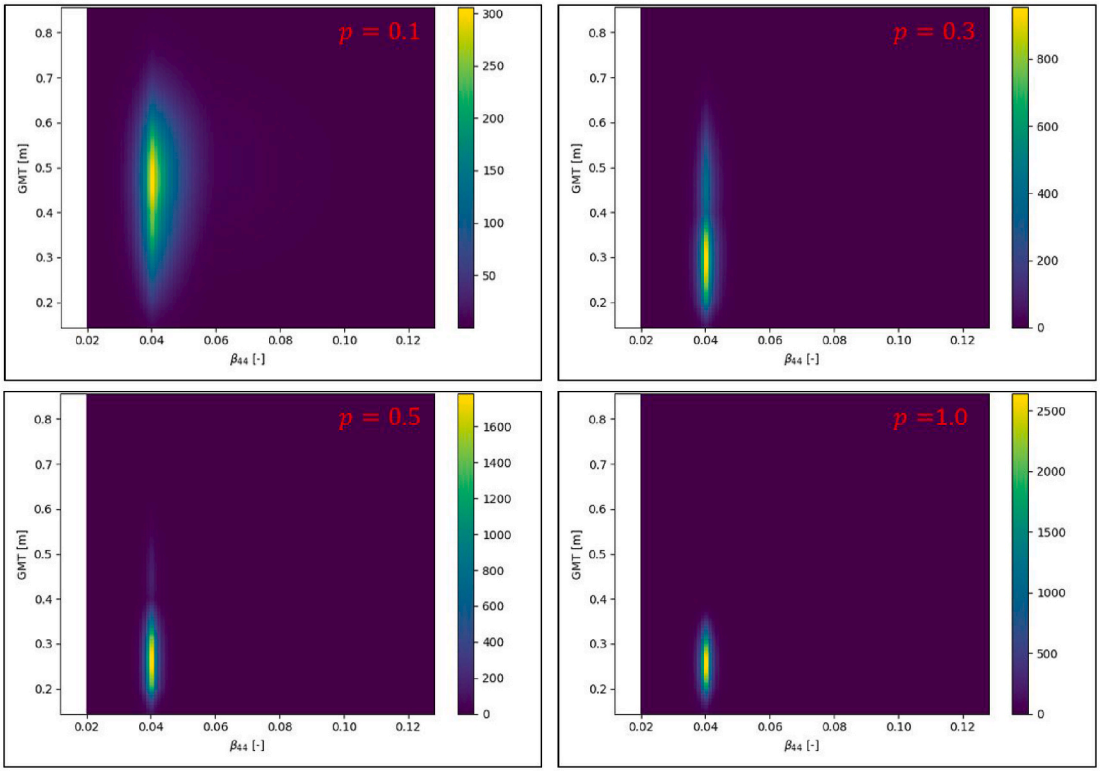

Fig. 11. Parameter tuning results from sea states in Table 4 for different power parameters.

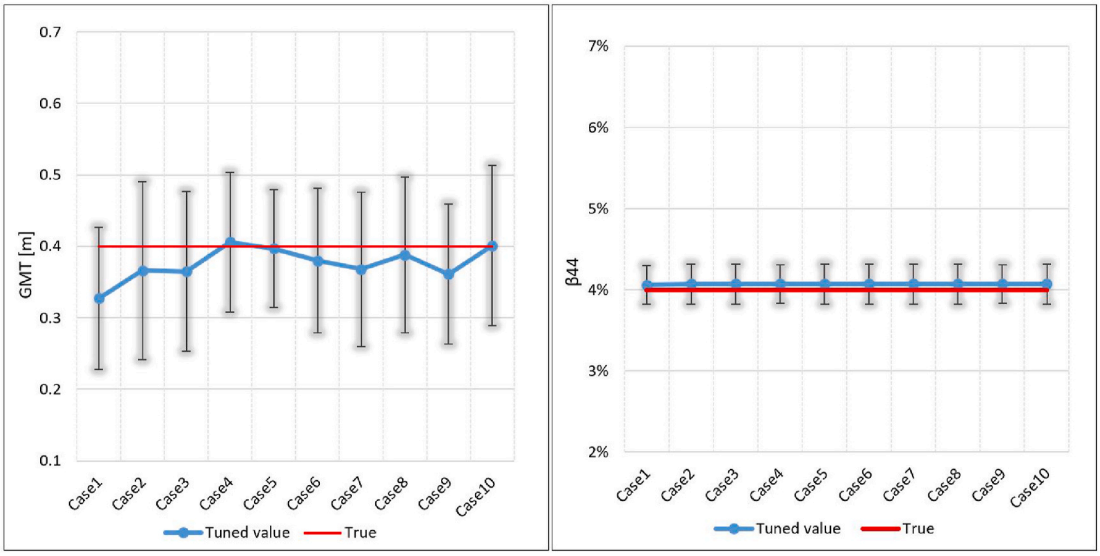

Fig. 12. Variation of tuned GMT and β_{44} due to seed variation, error bars indicate $\pm 1\sigma$.

Table 13
Sensitivity with respect to f_{lp} - tuning GMT [m] and β_{44} [-].

f_{lp} [Hz]	μ_{GMT}	σ^2_{GMT}	$\mu_{\beta_{44}}$	$\sigma^2_{\beta_{44}}$
0.2	0.411	0.004	0.0406	4.73E-06
0.33	0.386	0.0113	0.0407	5.92E-06
0.5	0.384	0.0118	0.0407	5.97E-06
1.0 (Base case)	0.353	0.0128	0.0407	5.85E-06
1.5	0.368	0.0150	0.0407	6.00E-06
2.0	0.318	0.0117	0.0406	5.86E-06

5.5. Sensor screening ratio - α

The selection of α depends on the uncertainty ranges of the considered parameters, and the uncertainties from input such as waves and response measurements. For a given uncertainty range of parameters, larger α leads to model tuning with less valuable sensor data, which may slow down the convergence speed. Smaller α helps to tune the model with more sensor data, but on the other hand, may lead to wrong results because the noise cannot be always perfectly treated.

Table 15 shows how the tuned results vary with α. It is clear that when α is reduced, more sensors which are less influenced by the considered uncertain vessel hydrodynamic parameters are included. Due to noise, the filtered signal variance deviates from the true response variance. If the noise was not appropriately filtered, those less important sensors generally would accelerate the tuning to a deviated value. Therefore, it is important to ensure a good selection of f_{lp} value, or acquire some additional knowledge on the noise and uncertainties. Based on Section 5.4, $f_{lp} = 0.2$ Hz suits better for the case study. Therefore, a sensitivity of α with respect to the lowpass filter cutoff frequency of 0.2 Hz was also studied, as shown in Table 16. With better handling of noise, more sensors were used with smaller α, generally leading to better model tuning results. Therefore, a trade-off between α and f_{lp} should be considered for practical purposes, due to the existence of uncertainties and limitations of noise filtering.

Table 14
Sensitivity with respect to f_{lp} - tuning XCG [m] and mass [t].

f_{lp} [Hz]	μ_{XCG}	σ^2_{XCG}	μ_{mass}	σ^2_{mass}
0.20	57.70	0.248	12099	62368
0.33	57.81	0.314	12131	62498
0.5	57.82	0.322	12137	60358
1.0 (Base case)	57.84	0.334	12145	58806
1.5	57.86	0.346	12149	58758
2.0	57.87	0.356	12155	57998

6. Validation and robustness

So far, only two 2-dimensional model tuning cases have been studied, for 5 sea states. In order to validate the proposed tuning approach, more extensive hydrodynamic model tuning analyses were carried out. For one selected true vessel condition, sensor signals were simulated for 6 sea states. The duration for each sea state was 1 hour. Parameters defining the sea states (i.e., H_s, T_z, β_W and seed) were randomly selected within the range described in Table 17. GMT, r_{55}, XCG and β_{44} were selected for model tuning. The reason to exclude mass coefficient was because the results from Section 4.2 indicate that the vessel mass does not have a significant influence within its considered uncertainty range. The validation analyses included 120 tuning results. All 4 parameters were tuned simultaneously.

Tuning 4 parameters at the same time became slower compared with the previous cases of tuning 2 parameters. Therefore, the power

Table 15
Sensitivity with respect to SSR α with $f_{lp} = 1.0$ Hz - tuning GMT [m] and β_{44} [-].

α	μ_{GMT}	σ^2_{GMT}	$\mu_{\beta_{44}}$	$\sigma^2_{\beta_{44}}$	N_{out} [a]
0.01	0.294	0.0091	0.0408	4.98E-06	19
0.02	0.317	0.0106	0.0407	5.06E-06	22
0.05 (base case)	0.353	0.0128	0.0407	5.85E-06	26
0.1	0.339	0.0103	0.0408	7.53E-06	31
0.2	0.358	0.0108	0.0413	1.65E-05	36

[a] Number of sensors screened out. For each study, there were 45 sensor data (5 sea states × 9 sensors).

Table 16
Sensitivity with respect to SSR α with $f_{lp} = 0.2$ Hz - tuning GMT [m] and β_{44} [-].

α	μ_{GMT}	σ^2_{GMT}	$\mu_{\beta_{44}}$	$\sigma^2_{\beta_{44}}$	N_{out} [a]
0.01	0.401	0.0026	0.0405	3.76E-06	19
0.02	0.4	0.0032	0.0406	4.08E-06	21
0.05 (base case)	0.411	0.004	0.0406	4.73E-06	25
0.1	0.426	0.0046	0.0407	6.77E-06	31
0.2	0.418	0.0042	0.0411	1.33E-05	36

[a] Number of sensors screened out. For each study, there were 45 sensor data (5 sea states × 9 sensors).

Table 17
Applied parameters related to the model tuning process for method validation.

Parameter	Value
H_s	Uniformly distributed in [1.0, 3.0] m
T_z	Uniformly distributed in [4.0, 15.0] s
β_W	Randomly selected among 13 discrete values $\beta_W \in \{0°, 15°, \ldots, 180°\}$
Seed	Randomly generated
Duration	3600 s
SNR	50
f_{lp}	0.2 Hz
α	0.05
p	0.4

parameter p was increased to 0.4. The joint probability distribution of the parameters was initiated as shown in Table 18. The key parameters needed for sensor signal generation and the tuning methodology are summarized in Table 17.

Due to limited computational processing capacity of the available laptop (CPU Intel(R) TM i7-8650U @ 1.90 GHz, 32 GB memory), a limited number of discretized values had to be applied for each parameter. To tune 4 parameters, the acceptable total number of discrete combinations was below 1.3E+07. This might be due to the large memory demands from Python Numpy operations during 4-dimensional interpolation of the calculated weight matrices described in Section 2.6. The computational capacity can be increased by optimizing the codes, changing the data structure, or simply increase the computer memory capacity. Table 18 describes the applied number of discrete parameter values for the joint probability distribution. The resolution for the uncertain parameters is considered sufficient with respect to the studied parameter ranges. For tuning a 4-dimensional model, with the considered uncertain range and resolution, the computational time for each sea state was about 90 s. For the 2-dimensional tuning model with 100×100 resolution for the probability distribution, the computational time for each sea state was about 10 s.

Table 18
Prior information and true values of the considered vessel parameters.

Parameter	Mean	σ^2	$\pm 3\sigma$	True value	N_{prob} [a]	N_{RAO} [b]
GMT [m]	0.5	0.015	[0.13, 0.87]	0.4	40	6
β_{44}	0.07	4.0E-04	[1%, 13%]	0.04	50	7
r_{55} [·m]	32.5	1.0	[29.5, 35.5]	30.55	30	7
XCG [m]	59.4	1.21	[56.1,62.7]	61.4	30	5

[a] Number of discrete variable values for the joint probability model.
[b] Number of discrete parameter values used in the RAO database.

From Figs. 13 and 14, it is clear that the proposed tuning procedure succeeds to tune β_{44} and XCG in most cases. However, a large variation of tuning results for GMT and r_{55} were also experienced. This is consistent with the findings from the earlier hydrodynamic parametric sensitivity studies (Han et al., 2020), showing that the vessel RAO is much less sensitive to GMT and r_{55} compared to β_{44} and XCG. For illustration purposes, each figure only contains information on 2 parameters.

Similar to all other experiment or test calibration methodologies (e.g., machine learning algorithms, hydrodynamic coefficients fitted based

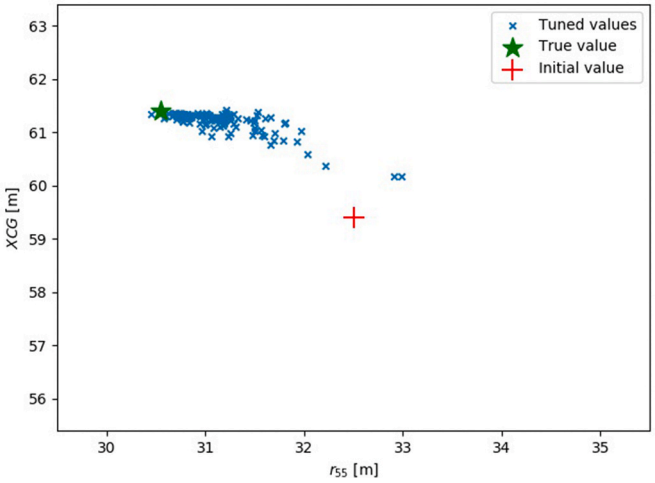

Fig. 14. Tuning results for validation analyses, expected values of r_{55} and XCG.

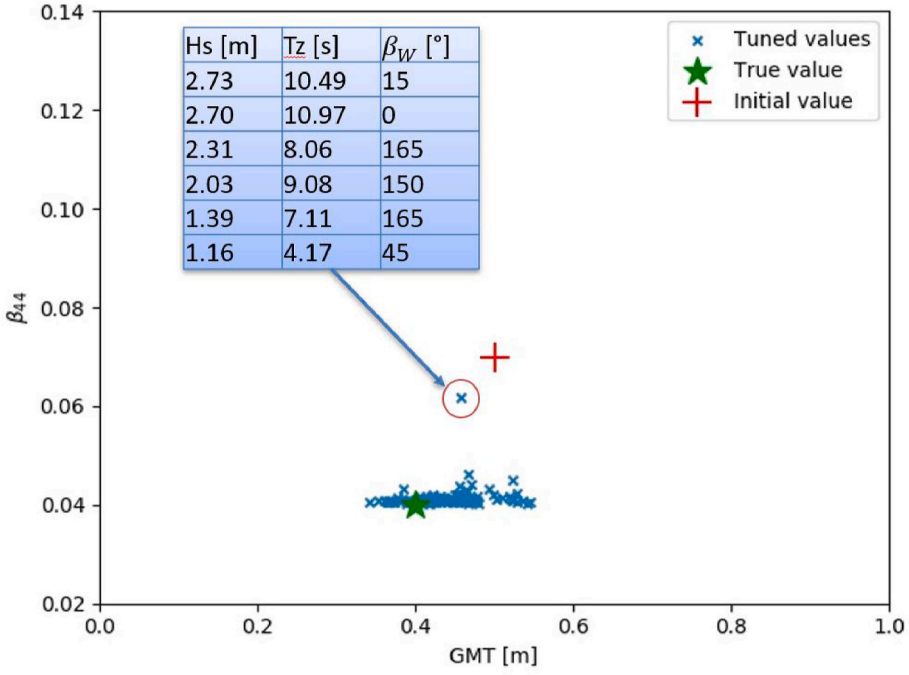

Fig. 13. Tuning results for validation analyses, expected values of GMT and β_{44}.

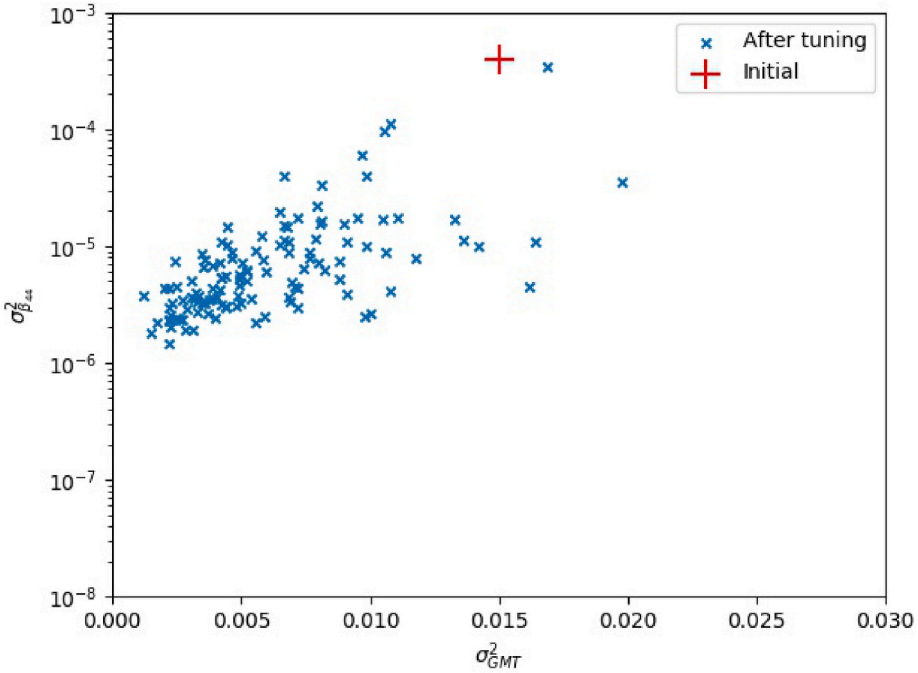

Fig. 15. Tuning results for validation analyses, variance of GMT and β_{44}.

on laboratory tests), relevant and valuable cases (sea states) are required in order to tune the parameters. But different from the complex AI algorithms like neural networks, the physics-based model tuning is better at extrapolation from the available data and does not require a huge amount of data samples. This is particularly important for nonlinear problems. Extrapolation here means good vessel response predictions for outlier sea states. The process for tuning hydrodynamic parameters still requires that the available RAO database covers the entire range of hydrodynamic parameter uncertainties. The validation analyses were limited to only 6 sea states for each tuning. Therefore, failure of model tuning is, by nature, possible. For example, one out of the 120 tuning simulations failed to report good enough additional roll damping, highlighted in Fig. 13. A deep investigation showed that all the generated sensor signals were basically from head and following sea states where β_{44} played a negligible role, and none of the sea states were near the roll resonance period.

Figs. 15 and 16 illustrate how the variance changes after tuning. Analyses show that the variable variance significantly reduces after tuning especially for the important parameters (i.e., β_{44} and XCG), as expected. Note that the y-axis of Fig. 15 is log-scaled.

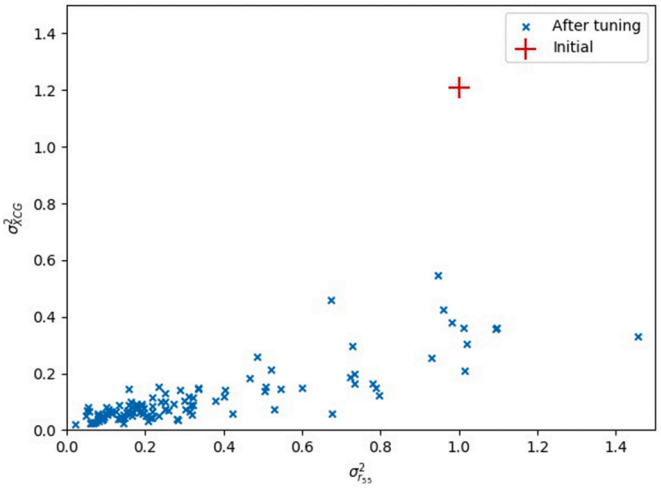

Fig. 16. Tuning results for validation analyses, variance of r_{55} and XCG.

Table 19
Summary of validation analyses results.

Parameter	Mean			Variance	
	Initial	Tuned	True	Initial	Tuned
GMT [m]	0.5	0.43	0.4	0.015	6.11E-03
β_{44}[-]	0.07	0.041	0.04	4.00E-04	1.26E-05
r_{55} [· m]	32.5	31.13	30.55	1.0	0.437
XCG [m]	59.4	61.2	61.4	1.21	0.141

The expected mean and variance of the parameters are summarized in Table 19. The tuning methodology succeeds to modify the parameters such that they approach the true values with significantly increased confidence. Therefore, the validation analyses demonstrated the robustness and stability of the proposed tuning methodology.

7. Conclusions and future work

A procedure with great potential for practical implementation with respect to tuning of vessel hydrodynamic seakeeping model parameters based on onboard vessel motion measurements has been proposed. Similar to model calibration based on laboratory tests, hydrodynamic coefficients can be modified based on available data by the tuning approach. Therefore, the improved vessel motion prediction is supported by physics and common engineering practice. But different from model calibration by laboratory tests, more uncertainties are in reality observed onboard. Therefore, it is more natural to present the important hydrodynamic parameters and RAOs in a probabilistic way. The proposed tuning approach combines engineering practice with the random nature, quantitatively improving the knowledge on the vessel conditions and response. Hence, the reliability of the vessel motion RAO and motion prediction can be documented quantitatively as well. Therefore, some of the safety factors in engineering practice related to marine operation design (e.g., DNVGL-ST-N001, 2016) may be reduced, and reliability-based marine operations may be possible. Consequently, the approach could potentially help to reduce the operational cost and

increase safety. The tuning process is fast and suitable for onboard application which could improve the quality of digital twins and assist within the context of onboard decision support.

Analyses demonstrate that the tuning approach is robust, and stable to deal with noise. Better tuning results were observed for the parameters which have stronger influence on the measured vessel response. The tuning algorithm also showed reasonable behaviour when updating the hydrodynamic parameters for cases where the sea states or the measurements were not very relevant for those uncertain parameters. Key parameters of the tuning methodology were also studied by sensitivity analyses. Relatively large values of the power parameter p led to higher belief in sensor data, and hence less memory to the prior knowledge. It was found important to select the cutoff frequency f_{lp} of the lowpass filter in a proper way for an unbiased tuning result. Practically, a trade-off between α and f_{lp} should be considered to optimally use the available measurement data. Inspired by Godhaven (1998), the lowpass filter cutoff frequency f_{lp} could be preferably modelled as sea state dependent, automatically selected based on measurements and environment information. The tuning methodology was also validated by using virtual sensor signals from randomly selected sea states by tuning 4 parameters simultaneously.

Even though a considerable amount of analyses were carried out for validation, more work is still required for methodology verification. Only one vessel condition was studied in Section 6. More vessel conditions and broader ranges of hydrodynamic parameters should be studied. More importantly, scaled experimental data and on-site full scale data should be used to verify the tuning methodology. The presented case studies of tuning vessel parameters (Fig. 1) and virtual sensor signal simulation (Fig. 3) apply the RAOs from the same RAO database which are generated based on seakeeping analyses by Wasim software. However, the real on-site vessel motion measurements will fully reflect the reality while the established RAO database to be used for vessel model tuning will be potentially subject to bias introduced by the simplifications made in the applied seakeeping software and the vessel numerical model. This software introduced bias should also be investigated in the future research work.

Practically, if the RAO database can be extended to various vessel advancing speeds with sufficient speed resolution, much more on-site measurements can be used to tune the important vessel parameters. Consequently, the cutoff frequency will therefore depend on vessel speed.

So far, the additional roll damping β_{44} was considered only operational condition dependent, which assumes a constant value throughout all sea states for the current vessel loading condition. Some parameters are sea state dependent (e.g., roll damping), some other parameters are operational condition dependent (such as inertia distribution), while others could be permanent (e.g., vessel geometry). Each parameter should be categorized accordingly and different model tuning strategy might be considered for each category.

So far, only uncertainties from sensor noise were considered. In reality, the uncertainties from wave information are significant, such as directional spreading, wave spectral shape, and uncertainties from wave forecast and hindcast modelling. Other environmental loads have not been considered, such as wind and current, leaving the procedure with a considerable gap towards on-site practice. Practically, these challenges can be solved by modifying the signal filter and by also including a highpass filter.

In addition, rigid body motion was assumed when calculating heave RAO functions at different locations. In reality for large slender vessels, more advanced models might therefore be required due to the increasing importance of hydroelastic effects.

CRediT authorship contribution statement

Xu Han: Conceptualization, Methodology, Software, Formal analysis, Data curation, Writing - original draft & Editing. **Bernt Johan Leira:** Writing - review & editing, Supervision, Project administration, Funding acquisition. **Svein Sævik:** Writing - review & editing, Supervision, Project administration.

Declaration of competing interest

The authors declare that they have no known competing financial interests or personal relationships that could have appeared to influence the work reported in this paper.

Acknowledgement

This work was made possible through the Center for Research based Innovation MOVE, financially supported by the the Research Council of Norway, NFR project No. 237929 and the consortium partners, http://www.ntnu.edu/move. Special thanks are given to Section of Hydrodynamics & Stability in DNV GL for providing hydrodynamic models and software support.

Nomenclature

$(\Phi_{i1},\ldots,\Phi_{iM})$ The combination of variable values from the $i1^{th}$ value of Φ_1,$i2^{th}$ value of Φ_2, …, and the iM^{th} value of Φ_M. $im \in [1,Im]$, Im is the number of discrete values for Φ_m in the RAO database, $m \in [1,M]$

$(\Phi_{k1},\ldots,\Phi_{kM})$ The combination of variable values from the $k1^{th}$ value of Φ_1, $k2^{th}$ value of Φ_2, …, and the kM^{th} value of Φ_M. $km \in [1,Km]$, Km is the number of discrete values for Φ_m in the joint distribution model, $m \in [1,M]$

α_j Sensor screening ratio (SSR) for sensor j

β_{44} Ratio between the additional roll damping and the critical roll damping. The additional damping can be expressed as $\beta_{44} \cdot \beta_{cr,44} = \beta_{44} \cdot 2\sqrt{(\overline{\overline{A}}(\omega_e)+\overline{\overline{M_0}})\cdot\overline{\overline{C}}}$

β_W Wave direction with respect to. vessel coordinate system

$\eta_{33},\dot{\eta_{33}},\ddot{\eta_{33}}$ Heave displacement, velocity, acceleration

$\widehat{\sigma}_j$ Standard deviation of the filtered signal from sensor j

$\widehat{x}_j(t)$ Filtered signal from sensor j

μ Variable mean value

ω Wave frequency

ω_e Encounter frequency

ω_p Spectral peak frequency, $\omega_P = 2\pi/T_p$

$\overline{\overline{\beta}}$ Vessel damping matrix

$\overline{\overline{A}}$ Vessel added mass matrix

$\overline{\overline{C}}$ Vessel restoring stiffness matrix
$\overline{\overline{M_0}}$ Vessel inertia matrix
$\overline{\overline{W_j}}$ Weight matrix based on measurement from sensor j
Φ Random variable
σ_N^2 Variance of noise
σ_X^2 Variance of response
$\sigma_{r,j}^*$ The predicted standard deviation by using $RAO_{r,j}$
$\sigma_{\sigma_{r,j}^*}$ The standard deviation of $\sigma_{r,j}^*$ over $r \in \{1, 2, \ldots, R\}$
ϕ Phase angle
ζ Wave elevation
B Vessel breadth
$C(\omega)$ The amplitude of the sinusoidal response at frequency of ω
D Vessel draft
f_{lp} Lowpass filter cutoff frequency in Hz
$H_{33}(\omega, \beta_W)$ Heave motion RAO
$H_{r,X_j\zeta}(\omega, \beta_W)$ Linear transfer function between wave and vessel response at sensor j based on r^{th} combination of uncertain vessel parameters
H_s Significant wave height
r_{55} Radius of gyration for pitchn
Im The total number of discrete values for Φ_m in the RAO database
im The im^{th} value of the variable in the RAO database for Φ_m
J The number of sensors
j Sensor ID, the j[th] sensor, representing different quantities (displacement, velocity, acceleration) and locations
Km The number of discrete values for Φ_m in the joint probability distribution
km The km^{th} value of the discretized variable in the probability distribution model for Φ_m
L_{PP} Length between perpendiculars
M The number of considered variables for tuning
N_ω The number of discretized frequencies
N_t The number of discretized time steps
p Power parameter
$P^{(n)}(\Phi_1, \ldots, \Phi_M)$ The updated discrete joint probability distribution after the n^{th} updating step
R The total number of possible combinations of uncertain vessel parameters in the RAO database
$RAO_{r,j}$ The RAO based on the variable combination r, corresponding to the response sensor j (location and quantity)
$S_{\zeta\zeta}^+(\omega, \beta_W)$ Single-sided power spectral density of waves
$S_{r,X_jX_j}^+(\omega)$ Calculated single-sided power spectral density of vessel response at sensor j based on RAO candidate $RAO_{r,j}$
$S_{X_jX_j}^+(\omega)$ Single-sided power spectral density of vessel response at sensor j
T_p Spectral peak period, $T_p = 1.4049T_z$ for PM spectrum (DNVGL-RP-C205, 2017)
T_z Zero-upcrossing wave period
u Vessel speed
$w_{r,j}$ Weight factor for the r^{th} variable combination based on measurement from sensor j
$x_j(t)$ Signal from sensor j
$\overrightarrow{F}(\omega, u|\beta_W)$ Excitation force from waves including Froude-Krylov and diffraction forces
AI Artificial intelligence
CFD Computational fluid dynamics
COG Center of gravity
DOF Degree of freedom
FFT Fast Fourier transform
GMT Free surface correction to the transverse metacentric height
ODSS Onboard decision support system
OSV Offshore supply vessel
PDF Probability density function
PM Pierson-Moskowitz spectrum
RAO Response amplitude operator
SNR Signal-to-noise ratio
SS Sea state
SSR Sensor screening ratio
XCG Longitudinal coordinate of vessel COG
YCG Transverse coordinate of vessel COG
ZCG Vertical coordinate of vessel COG

References

Alford, L.K., Beck, R.F., Johnson, J.T., Lyzenga, D., Nwogu, O., Zundel, A., 2014. Design, Implementation, and Evaluation of a System for Environmental and Ship Motion Forecasting. Proceedings of the 30th Symposium on Naval Hydrodynamics. Hobart, Australia.

Alford, L.K., Beck, R.F., Johnson, J.T., Lyzenga, D., Nwogu, O., Zundel, A., 2015. A real-time system for forecasting extreme waves and vessel motions. Proceedings of the ASME 2015 34th International Conference on Ocean, Offshore and Arctic Engineering, 11. Newfoundland, Canada.

Brodtkorb, A.H., Nielsen, U.D., Sørensen, A.J., 2018b. Online wave estimation using vessel motion measurements. IFAC-PapersOnLine 51 (29), 244–249. https://doi.org/10.1016/j.ifacol.2018.09.510. ISSN 2405–8963, 11th IFAC Conference on Control Applications in Marine Systems, Robotics, and Vehicles CAMS 2018.

Brodtkorb, A.H., Nielsen, U.D., Sørensen, A.J., 2018a. Sea state estimation using vessel response in dynamic positioning. Appl. Ocean Res. 70, 76–86. https://doi.org/10.1016/j.apor.2017.09.005. ISSN 0141–1187.

Cao, Y., Tahchiev, G., Zhang, F., Aarsnes, J.V., Glomnes, E.B., 2010. Effects of Hydrostatic Nonlinearity on Motions of Floating Structures. Proceedings of the ASME 2010 29th International Conference on Ocean, Offshore and Arctic Engineering, 4. Shanghai, China.

Cheng, X., Li, G., Skulstad, R., Major, P., Chen, S., Hildre, H.P., Zhang, H., 2019. Data-driven uncertainty and sensitivity analysis for ship motion modeling in offshore operations. Ocean. Eng. 179, 261–272. https://doi.org/10.1016/j.oceaneng.2019.03.014. ISSN 0029–8018.

Clauss, G.F., Kosleck, S., Testa, D., 2012. Critical Situations of Vessel Operations in Short Crested Seas - Forecast and Decision Support System. Journal of Offshore Mechanics and Arctic Engineering 134.

Connell, B.S.H., Rudzinsky, J.P., Brundick, C.S., Milewski, W.M., Kusters, J.G., Farquharson, G., 2015. Development of an Environmental and Ship Motion Forecasting System. Proceedings of the ASME 2015 34th International Conference on Ocean, Offshore and Arctic Engineering. Newfoundland, Canada.

Dannenberg, J., Hessner, K., Naaijen, P., van den Boom, H., Reichert, K., 2010. The on board wave and motion estimator OWME. In: Proceedings of the 20th International Offshore and Polar Engineering Conference. ISOPE, pp. 424–431. ISBN 978-1-880653-77-7.

De Masi, G., Gaggiotti, F., Bruschi, R., Venturi, M., 2011. Ship motion prediction by radial basis neural networks. In: IEEE Workshop on Hybrid Intelligent Models and Applications. IEEE, Paris, France, pp. 28–32. ISSN 2167-8219.

DNV GL, 2018. Wasim User Manual. Tech. Rep. DNV GL.

DNVGL-RP-C205, 2017. Environmental Conditions and Environmental Loads. Tech. Rep. DNV GL.

DNVGL-ST-N001, 2016. Marine Operations and Marine Warranty. Tech. Rep. DNV GL.

Faltinsen, O.M., 1990. Sea Loads on Ships and Offshore Structures. Cambridge University Press Cambridge, New York. ISBN 0521372852 0521458706.

Faltinsen, O.M., 2015. Hydrodynamics of marine and offshore structures. Journal of Hydrodynamics, Ser. B 26 (6), 835–847.

Galvin, J., 2014. The Use of Information Technology at the Met Office. British Computer Society, Bristol Branch January Seminar.

Godhaven, J.-M., 1998. Adaptive tuning of heave filter in motion sensor. In: IEEE Oceanic Engineering Society. OCEANS'98. Conference Proceedings (Cat. No.98CH36259), vol. 1. IEEE, pp. 174–178.

Grilli, S.T., Guérin, C.-A., Goldstein, B.I., 2011. Ocean Wave Reconstruction Algorithms Based on Spatio-Temporal Data Acquired by a Flash LIDAR Camera. International Society of Offshore and Polar Engineers, Hawaii, USA.

Han, X., Sævik, S., Leira, B.J., 2020. A sensitivity study of vessel hydrodynamic model parameters. Proceedings of the ASME 2020 39th International Conference on Ocean, Offshore and Arctic Engineering. Virtual, Online, OMAE2020-19039.

Himeno, Y., 1981. Prediction of Ship Roll Damping - A State of the Art. Tech. Rep. The University of Michigan, College of Engineering, Department of Naval Architecture and Marine Engineering, USA.

Hoyer, S., Hamman, J., 2017. xarray: N-D labeled Arrays and Datasets in Python. Journal of Open Research Software 5 (1), 10. http://doi.org/10.5334/jors.148.

Iseki, T., 2009. Real-time estimation of directional wave spectra using non-stationary ship motion data. In: Proceedings of the ASME 2009 28th International Conference on Ocean, Offshore and Arctic Engineering, pp. 673–678. https://doi.org/10.1115/OMAE2009-79295.

Kim, S.P., 2011. CFD as a seakeeping tool for ship design. International Journal of Naval Architecture and Ocean Engineering 3 (1), 65–71. https://doi.org/10.2478/IJNAOE-2013-0046. ISSN 2092–6782.

Kring, D.C., 1994. Time Domain Ship Motions by a Three-Dimensional Rankine Panel Method. Ph.D. thesis. Massachusetts Institute of Technology, Department of Ocean Engineering.

Kusters, J.G., Cockrell, K.L., Connell, B.S.H., Rudzinsky, J.P., Vinciullo, V.J., 2016. FutureWavesTM: a real-time ship motion forecasting system employing advanced wave-sensing radar. In: OCEANS 2016 MTS/IEEE Monterey. IEEE, pp. 1–9.

Labbe, R., 2018. Kalman and Bayesian Filters in Python.

Larsen, C.M., Lian, W., Bachynski, E., Kristiansen, T., Myrhaug, D., 2019. Lecture Notes for Course TMR4182 Marine Dynamics. Tech. Rep. Department of Marine Technology, NTNU, Trondheim.

Milewski, W.M., Connell, B.S.H., Vinciullo, V.J., Kirschner, I.N., 2015. Reduced Order Model for Motion Forecasts of One or More Vessels. Proceedings of the ASME 2015 34th International Conference on Ocean, Offshore and Arctic Engineering, 11. Newfoundland, Canada.

Naaijen, P., Roozen, D.K., Huijsmans, R.H.M., 2016. Reducing Operational Risks by On-Board Phase Resolved Prediction of Wave Induced Ship Motions. Proceedings of the ASME 2016 35th International Conference on Ocean, Offshore and Arctic Engineering, 7. Busan, South Korea.

Naaijen, P., van Oosten, K., Roozen, K., van't Veer, R., 2018. Validation of a Deterministic Wave and Ship Motion Prediction System. Proceedings of the ASME 2018 37th International Conference on Ocean, Offshore and Arctic Engineering, 7B. Madrid, Spain.

Nielsen, U.D., 2006. Estimations of on-site directional wave spectra from measured ship responses. Mar. Struct. 19 (1), 33–69. https://doi.org/10.1016/j.marstruc.2006.06.001. ISSN 0951–8339.

Nielsen, U.D., 2007. Response-based estimation of sea state parameters - influence of filtering. Ocean. Eng. 34 (13), 1797–1810. https://doi.org/10.1016/j.oceaneng.2007.03.002. ISSN 0029–8018.

Nielsen, U.D., 2017. Transformation of a wave energy spectrum from encounter to absolute domain when observing from an advancing ship. Appl. Ocean Res. 69, 160–172. https://doi.org/10.1016/j.apor.2017.10.011. ISSN 0141–1187.

Nielsen, J.K., Pedersen, N.H., Michelsen, J., Nielsen, U.D., Baatrup, J., Jensen, J.J., Petersen, E.S., 2006. SeaSense - real-time onboard decision support. In: World Maritime Technology Conference. London, UK.

Nielsen, U.D., Brodtkorb, A.H., Jensen, J.J., 2018. Response predictions using the observed autocorrelation function. Mar. Struct. 58, 31–52. https://doi.org/10.1016/j.marstruc.2017.10.012. ISSN 0951–8339.

Nielsen, U.D., Brodtkorb, A.H., Sørensen, A.J., 2019. Sea state estimation using multiple ships simultaneously as sailing wave buoys. Appl. Ocean Res. 83, 65–76. https://doi.org/10.1016/j.apor.2018.12.004. ISSN 0141–1187.

Nouguier, F., Grilli, S.T., Guérin, C., 2014. Nonlinear ocean wave reconstruction algorithms based on simulated spatiotemporal data acquired by a flash LIDAR camera. IEEE Trans. Geosci. Rem. Sens. 52 (3), 1761–1771. https://doi.org/10.1109/TGRS.2013.2254494. ISSN 1558–0644.

Ren, Z., Han, X., Verma, A.S., Dirdal, J.A., Skjetne, R., 2021. Sea state estimation based on vessel motion responses: improved smoothness and robustness using Bézier surface and L1 optimization. Mar. Struct. In press.

Shepard, D., 1968. A two-dimensional interpolation function for irregularly-spaced data. In: Proceedings of the 1968 23rd ACM National Conference, ACM '68. Association for Computing Machinery, New York, NY, USA, pp. 517–524. ISBN 9781450374866.

Tannuri, E.A., Sparano, J.V., Simos, A.N., Da Cruz, J.J., 2003. Estimating directional wave spectrum based on stationary ship motion measurements. Appl. Ocean Res. 25 (5), 243–261. https://doi.org/10.1016/j.apor.2004.01.003. ISSN 0141–1187.

van Daalen, E., Fehribach, J., van Leeuwen, T., Reinhardt, C., Schenkels, N., Sheombarsing, R., 2014. Model calibration for ship simulations. In: Proceedings of the 98th Study Group Mathematics with Industry. TU Delft, pp. 68–91.

Yue, D.K., Liu, Y., Hendrickson, K., Wu, G., Xiao, W., Henry, L., 2008. Nonlinear Wave Environments for Ship Analysis. Proceedings of the 27th Symposium on Naval Hydrodynamics. Seoul, South Korea.